

Ignition conditions for magnetized target fusion in cylindrical geometry

M.M. Basko^{a*}, A.J. Kemp^b, J. Meyer-ter-Vehn^b

^a Département de Recherches sur la Fusion Contrôlée, CEA Cadarache, St. Paul-lez-Durance, France

^b Max-Planck-Institut für Quantenoptik, Garching, Germany

Abstract. Ignition conditions in axially magnetized cylindrical targets are investigated by examining the thermal balance of assembled DT fuel configurations at stagnation. Special care is taken to adequately evaluate the energy fraction of 3.5 MeV alpha particles deposited in magnetized DT cylinders. A detailed analysis of the ignition boundaries in the $\rho R, T$ parametric plane is presented. It is shown that the fuel magnetization allows a significant reduction of the ρR ignition threshold only when the condition $BR \gtrsim 6 \times 10^5$ G cm is fulfilled (B is the magnetic field strength and R is the fuel radius).

1. Introduction

Magnetized target fusion (MTF) is inertial confinement fusion (ICF) with a magnetic field introduced into the deuterium–tritium (DT) fuel. The role of the magnetic field is to reduce the heat conduction losses from the DT plasma and to retain the 3.5 MeV alpha particles. The direct impact of magnetic pressure on the implosion hydrodynamics and duration of the stagnation phase is typically negligible.

The MTF concept has been discussed in the literature mostly in the context of spherical implosions [1–4], and to a lesser extent for cylindrical geometry [5–7]. In this article we focus our attention on magnetized DT cylinders. The interest in a cylindrical MTF stems from the following considerations. First of all, the cylindrical geometry is generally better suited for the introduction of an external magnetic field. In addition, strong motivation comes from inertial fusion driven by heavy ion beams. For relatively rigid ion beams, which are accelerated, stored and transported along extended horizontal structures, a cylindrical symmetry of target irradiation may be easier to achieve than the spherical one. Ion driven magnetized cylindrical targets could possibly even be envisaged in direct drive schemes for inertial fusion energy [5].

In the context of the ignition problem, the principal objective of introducing a magnetic field into ICF targets is to reduce the threshold value of the fuel ρR at ignition. In the first place, this is necessitated by the cylindrical geometry itself because, under similar constraints on drive pressure uniformity and Rayleigh–Taylor instability, cylindrical implosions are less efficient in compressing fuel than spherical ones [7]. Secondly, by lowering the fuel ρR at ignition one can reduce considerably the required driver power — a particularly sensitive issue for a heavy ion driver.

The latter point can be illustrated by the following simple scaling law observed for a quasi-uniform DT cylinder imploded by a massive liner of mass M_l (g/cm). The total energy (per unit length) of this simple configuration can be written as

$$E = \frac{1}{2} M_l v_{im}^2 = \frac{3\pi}{2} P R^2 \quad (1)$$

where v_{im} is the implosion velocity, and R and P are the fuel radius and the pressure at stagnation, respectively. By using Eq. (1), we can relate the time of inertial confinement around the moment of stagnation,

$$t_c \propto \left(\frac{M_l}{P} \right)^{1/2} \propto \frac{R}{v_{im}} \approx \frac{t_{im}}{C_r} \quad (2)$$

to the implosion time $t_{im} \approx R_0/v_{im}$, where R_0 is the initial fuel radius and $C_r = R_0/R$ is the radial

* *On leave from:* Institute for Theoretical and Experimental Physics, Moscow, Russian Federation.

convergence ratio. If we invoke now the break-even condition

$$\frac{1}{4}n^2\langle\sigma v\rangle_{DT}E_{DT}t_c = 3nT \quad (3)$$

to evaluate t_c , we obtain the following scaling for the required driver power:

$$W_{dr} \propto \frac{E}{t_{im}} \propto \frac{PR^2}{C_r t_c} \propto \frac{(\rho R)^2}{C_r} \langle\sigma v\rangle_{DT}. \quad (4)$$

In Eq. (3) n is the ion number density at peak compression, $E_{DT} = 17.6$ MeV is the DT reaction energy and the reaction rate $\langle\sigma v\rangle_{DT}$ is a function of temperature T only. Equation (4) tells us that, for a fixed ignition temperature T (which is typically close to 10 keV), the driver power W_{dr} scales as the square of the fuel ρR at the ignition threshold.

In this article we investigate the ignition conditions in stagnating uniformly magnetized DT cylinders. Neither the implosion dynamics nor the problem of confinement are considered here, and only the thermal balance of assembled fuel configurations is analysed. The hot DT region is supposed to be tamped by a cold wall of either dense fuel or external liner material. Although the tamper properties do not appear explicitly in the following analysis, their presence is tacitly assumed to provide a sink for the energy carried away by the heat conduction out of the hot DT core. Our main conclusion is that a significant reduction in the fuel ρR at the ignition threshold is only possible when the 3.5 MeV alpha particles become at least marginally magnetized, so that their Larmor radius $r_{\alpha L} \simeq R$. The latter implies an ignition threshold of $\simeq 6 \times 10^5$ G cm for the product BR , where B is the magnetic field strength in the compressed state.

2. Energy deposition by alpha particles

In this section we calculate the energy fraction of the 3.5 MeV alpha particles, f_α , deposited due to Coulomb collisions with plasma electrons in a uniformly magnetized DT cylinder of radius R embedded into a uniform magnetic field B directed along the cylinder axis. In such a problem, the dimensionless quantity $0 < f_\alpha < 1$ is a function of two dimensionless parameters, which we choose to be

$$\bar{R} = \frac{R}{l_\alpha}, \quad b = \frac{R}{r_{\alpha L}} = R \frac{\omega_\alpha}{v_{\alpha 0}}. \quad (5)$$

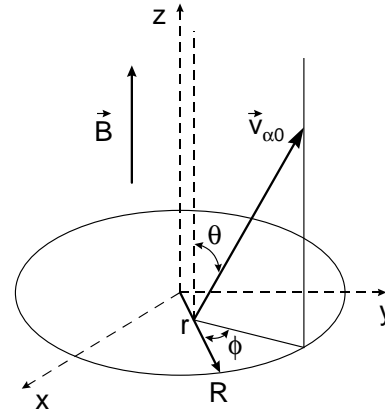


Figure 1. Co-ordinate system used in Section 2.1 for calculating the alpha energy deposition fraction f_α .

Here l_α is the Coulomb range of the alpha particles, $r_{\alpha L}$ is their Larmor radius at the birth velocity $v_{\alpha 0} = 1.3 \times 10^9$ cm/s and

$$\omega_\alpha = \frac{2eB}{m_\alpha c} \quad (6)$$

is their Larmor frequency. We consider the entire variation range of $0 < \bar{R}, b < \infty$, with a particular interest for the case of $\bar{R} \ll 1$.

2.1. Method of calculation

We assume that the Coulomb collisions decelerate alphas by means of dynamic friction only, and that diffusion in velocity space can be neglected. The friction force is supposed to be directly proportional to the velocity of the alphas, which is a reasonable approximation for plasma temperatures $1 \text{ keV} \lesssim T \lesssim 20 \text{ keV}$ [8]. Then, the equations of motion for an individual alpha particle become

$$\begin{aligned} \dot{v}_x &= \omega_\alpha v_y - \nu_\alpha v_x \\ \dot{v}_y &= -\omega_\alpha v_x - \nu_\alpha v_y \end{aligned} \quad (7)$$

$$\dot{v}_z = -\nu_\alpha v_z$$

where dots denote the time derivative,

$$\nu_\alpha = \frac{v_{\alpha 0}}{l_\alpha} \quad (8)$$

is the effective collision frequency of the fast alphas, and the co-ordinate system is shown in Fig. 1 (the magnetic field B is along the z axis).

For the deceleration law given by Eqs (7), the fraction of the initial energy deposited by an individual alpha particle after it travels a distance s is given by

$$f_{\alpha s} = f_{\alpha s}(r, \theta, \phi) = 2 \left(\frac{s}{l_\alpha} \right) - \left(\frac{s}{l_\alpha} \right)^2. \quad (9)$$

Here r is the cylindrical radius of the alpha birth point, θ is the pitch angle and ϕ is the azimuthal angle (in the xy plane, with respect to the radius vector of the birth point) of the alpha birth velocity $v_{\alpha 0}$ (Fig. 1). In Eq. (9) $s = s(r, \theta, \phi)$ is the path length of an alpha particle with the birth parameters r, θ, ϕ before it either comes to a halt inside the cylinder or leaves the cylinder by crossing the boundary at $r = R$. In our calculations we assumed for simplicity that, once an alpha particle exits from the cylinder at $r = R$, it never returns. Any attempt to account for the re-entry of gyrating alphas should take into consideration the matter distribution outside the cylinder $r = R$, which would be beyond the scope of this work. Equations (7) imply that $s = l_{\alpha}[1 - \exp(-\nu_{\alpha}t)]$, and one only has to calculate by integrating Eqs (7) for the time t at which the particle with the birth parameters r, θ, ϕ exits from the cylinder $r = R$.

Once the function $f_{\alpha s}(r, \theta, \phi)$ is known, one calculates f_{α} by averaging $f_{\alpha s}$ from Eq. (9) over the angles θ, ϕ and the radius r ,

$$f_{\alpha} = \frac{2}{R^2} \int_0^R r dr \frac{1}{4\pi} \int_0^{\pi} \sin \theta d\theta \int_0^{2\pi} f_{\alpha s}(r, \theta, \phi) d\phi. \quad (10)$$

This approach is, of course, equivalent to solving the corresponding transport equation for the distribution function of alpha particles, as described for example in Ref. [9].

2.2. Asymptotical behaviour and numerical results

As a first step, consider the simplest case of $B = 0$ ($b = 0$), when the absorbed energy fraction f_{α} is a function of one parameter, $\bar{R} = R/l_{\alpha}$, only. In the case of a uniform sphere of radius R , all the integrals in Eq. (10) can be calculated analytically, with the result given in Ref. [10]. Not so for the cylinder: only the asymptotic behaviour in the limits of $\bar{R} \ll 1$ and $\bar{R} \gg 1$ can be established analytically,

$$f_{\alpha}(\bar{R}, b = 0) = \begin{cases} \frac{8}{3}\bar{R} + O(\bar{R}^2), & \bar{R} \ll 1, \\ 1 - \frac{1}{6\bar{R}} + O\left(\frac{1}{\bar{R}^2}\right), & \bar{R} \gg 1. \end{cases} \quad (11)$$

Next, we examine qualitatively the dependence of f_{α} on the magnetic field strength B in the limit of $R \ll l_{\alpha}$ ($\bar{R} \ll 1$). For this, all the alphas born inside the DT cylinder can be roughly divided into two groups, namely, those born at large pitch angles

$\theta \sim \pi/2$ (propagating nearly radially) and those born in the narrow ‘capture cone’ $0 < \theta \lesssim \theta_c \ll 1$, $0 < \pi - \theta \lesssim \theta_c \ll 1$. When $R \ll r_{\alpha L}$, all the ‘nearly radial’ alphas escape from the cylinder along almost straight trajectories, leaving a small fraction $f_{\alpha s} \sim \bar{R}$ of their initial energy in the DT plasma. The alphas born within the capture cone deposit all their energy in the DT cylinder, so that their contribution to f_{α} is proportional to the solid angle occupied by the capture cone, i.e. to θ_c^2 . The width of the capture cone can be readily evaluated as

$$\theta_c \sim \begin{cases} \frac{R}{l_{\alpha}}, & R \ll l_{\alpha} \ll r_{\alpha L} \\ \frac{R}{r_{\alpha L}}, & R \ll r_{\alpha L} \ll l_{\alpha}. \end{cases} \quad (12)$$

As a result, we infer the following asymptotic behaviour for the total absorbed energy fraction

$$f_{\alpha}(\bar{R}, b) \sim \begin{cases} \frac{8}{3}\bar{R} + O(\bar{R}^2), & R \ll l_{\alpha} \ll r_{\alpha L} (b \ll \bar{R} \ll 1) \\ \frac{8}{3}\bar{R} + O(b^2), & R \ll r_{\alpha L} \ll l_{\alpha} (\bar{R} \ll b \ll 1) \\ 1 - O\left(\frac{1}{b}\right), & r_{\alpha L} \ll R \ll l_{\alpha} (\bar{R} \ll 1 \ll b). \end{cases} \quad (13)$$

In the last limit of a very strong magnetic field, $r_{\alpha L} \ll R$, only a small fraction of alphas born in a narrow surface layer of width $r_{\alpha L}$ escape from the DT cylinder.

The dependence of $f_{\alpha}(\bar{R}, b)$ on b , calculated by integrating numerically Eq. (10), is shown in Fig. 2, for three different values of \bar{R} . These calculations are in full agreement with the asymptotic formulas of Eqs (13). In particular, it is clearly seen that the transition from the ‘optically thin’ limit of $f_{\alpha} \approx \frac{8}{3}\bar{R} \ll 1$ in the non-magnetized case to a full absorption with $f_{\alpha} \approx 1$ in the limit of strong magnetization ($b \gg 1$) does indeed proceed along the intermediate asymptote

$$f_{\alpha} \propto b^2 \propto (BR)^2. \quad (14)$$

For practical applications, it is important to be aware of this intermediate asymptotic regime.

2.3. Approximate formula

For practical needs one would prefer to have a simple approximate formula for f_{α} . Here we propose

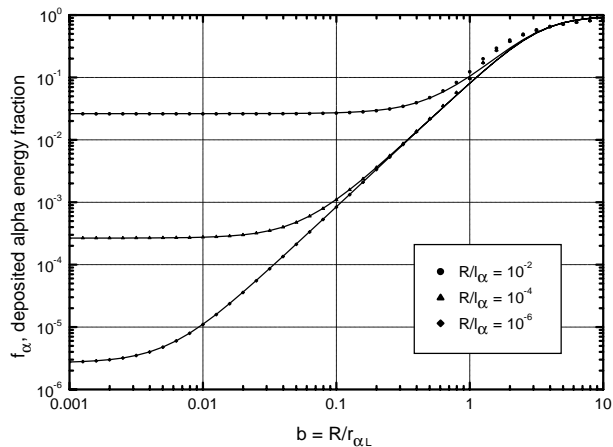


Figure 2. Energy fraction f_α , which the 3.5 MeV alpha particles deposit in a uniform magnetized DT cylinder, as calculated by performing the numerical integration in Eq. (10) (circles, triangles and diamonds). Approximate formula (15) is plotted with the solid curves. The three curves display the dependence of f_α on the dimensionless parameter b for three different values of \bar{R} (Eq. (5)).

the following expression appropriate for magnetized DT cylinders:

$$f_\alpha = \frac{x_\alpha + x_\alpha^2}{1 + 13x_\alpha/9 + x_\alpha^2} \quad (15a)$$

$$x_\alpha = \frac{8}{3} \left(\bar{R} + \frac{b^2}{\sqrt{9b^2 + 1000}} \right). \quad (15b)$$

For the zero magnetic field ($B = b = 0$) this formula conforms to both the limits in Eqs (11) and never deviates from the numerical results by more than 3.5% (for the quantity $1 - f_\alpha$ the maximum deviation amounts to 10%). The dependence on b in Eq. (15b) is chosen such as to describe both the limits of $b \ll 1$ and $b \gg 1$ as given by Eqs (13), and to fit the numerical results shown in Fig. 2. It has two numerical constants under the square root: the free term 1000 fits the numerical results along the intermediate asymptote (14), while the coefficient 9 of b^2 is chosen on the basis of the diffusion approximation (see Appendix).

The error of the formula (15) is very small (below 3%) whenever $f_\alpha < 0.05$, but may become as large as 50% for the values of $f_\alpha = 0.1$ –0.5. We did not try to improve the accuracy of Eq. (15) in the latter region, which corresponds to $R \simeq r_{\alpha L}$, because this would make little sense from the practical point of view due to the re-entry problem of the gyrating alpha particles. Note that the dependence $f_\alpha(\bar{R}, b)$ cannot

be adequately described (especially in the parameter region where $f_\alpha \ll 1$) by adopting the general recipe of reducing the alpha diffusion coefficient by the factor $1 + (\omega_\alpha/\nu_\alpha)^2$, as was for example assumed in Ref. [3].

A similar problem has been treated earlier by Gus'kov et al. [9] for a uniform sphere embedded in a uniform magnetic field. Such a situation is, however, qualitatively different from the one considered here: because each field line of the uniform B field pierces the spherical surface of the DT volume, the deposited alpha energy fraction $f_\alpha \sim \bar{R}$ remains small for $\bar{R} \ll 1$ even in the limit of an infinitely strong magnetic field. In our case, when the field lines run parallel to the surface of the DT volume, f_α approaches 1 in a sufficiently strong field for arbitrarily small $\bar{R} \ll 1$.

3. Lindl–Widner diagrams

The physical conditions that must be attained in the DT fuel to achieve ignition in ICF targets are best illustrated in the $\rho R, T$ parametric plane. An extensive discussion of the physical processes behind the $\rho R, T$ diagrams for non-magnetized DT microspheres was presented by Lindl [11]. Following Ref. [4], we call these diagrams the Lindl–Widner (LW) diagrams. An important fact is that, because the ignition condition can be expressed as a relationship between the two parameters T and ρR only, a single ignition curve in the $\rho R, T$ plane represents a two parameter family of similar fuel configurations having, for example, different temperatures and different masses.

Here we consider how the ignition boundary in the $\rho R, T$ plane for uniform DT cylinders at stagnation is influenced by the presence of a strong magnetic field. With one more parameter B to characterize the fuel state, we expect a single ignition boundary in the $\rho R, T$ plane to become a one parameter family of ignition curves. The topology of the ignition domain depends on the specific choice of the parameter (the ignition curve parameter), which is kept constant along each ignition curve. Figures 3 and 4 illustrate two distinct possibilities for the different topologies of the LW diagrams for the magnetized fuel.

In Fig. 3 the ignition curve parameter is taken to be the ratio B/ρ . This is a natural choice arising from the functional form of the Braginskii formulas [12] for the electron and ion heat conduction coefficients. The curves in Fig. 3 represent the fuel states for which the

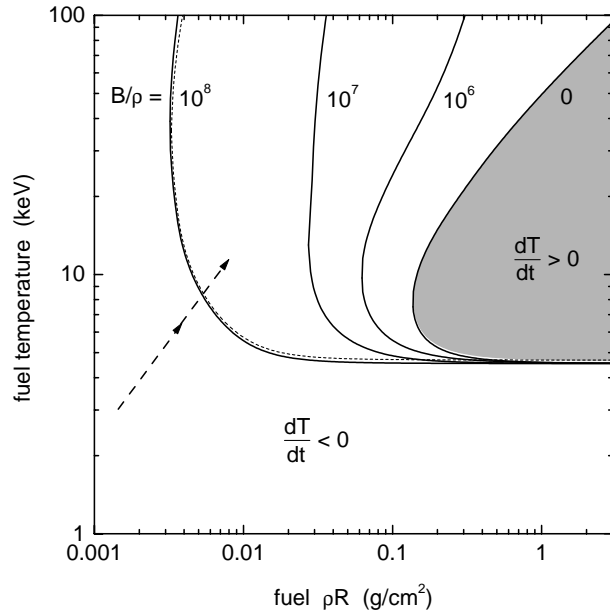


Figure 3. Lindl-Widner diagram for magnetized DT cylinders at stagnation. Solid curves show a series of ignition boundaries in the $\rho R, T$ plane calculated for four fixed values of the parameter B/ρ , given near each curve in units of $\text{G cm}^3/\text{g}$. The shaded area is the pure ICF ignition domain at $B = 0$. The dotted curve illustrates the effect of synchrotron radiation losses at $\rho = 1 \text{ g/cm}^3$, $B = 10^8 \text{ G}$. Dashed arrows indicate how the fuel states advance towards the ignition boundary in the process of a quasi-adiabatic implosion.

net heating rate

$$c_0 \frac{dT}{dt} = q_{tn} - q_{br} - q_c \quad (16)$$

is zero. Here

$$c_0 = 1.158 \times 10^{15} [\text{erg g}^{-1} \text{ keV}^{-1}] \quad (17)$$

is the heat capacity of the equimolar DT,

$$q_{tn} = 8.18 \times 10^{40} \rho \langle \sigma v \rangle_{DT} f_\alpha [\text{erg g}^{-1} \text{ s}^{-1}] \quad (18)$$

is the rate of the thermonuclear heating by the alpha particles,

$$q_{br} = 3.11 \times 10^{23} \rho T_{\text{keV}}^{1/2} [\text{erg g}^{-1} \text{ s}^{-1}] \quad (19)$$

is the rate of the bremsstrahlung cooling, and

$$q_c = \frac{2(\kappa_e + \kappa_i)T}{\rho R^2} \quad (20)$$

is the heat conduction energy loss. The heat balance equation (16) is written for a DT column surrounded by either a cold liner or a cold dense DT shell at the

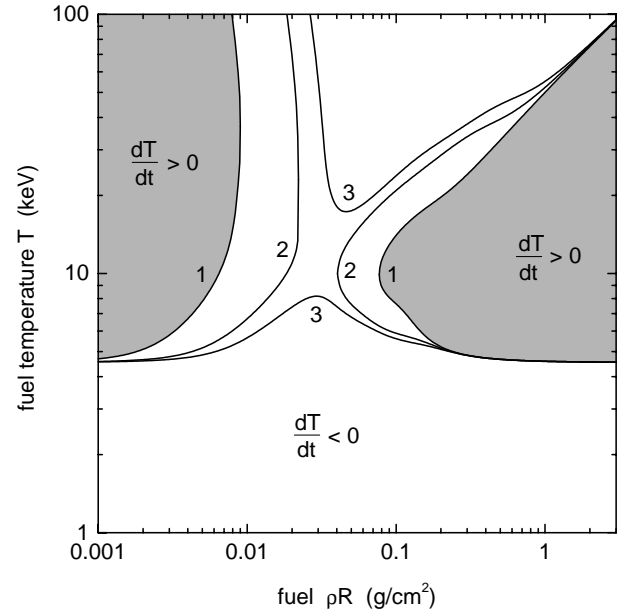


Figure 4. Alternative version of the LW diagram for magnetized DT cylinders. A series of ignition boundaries in the $\rho R, T$ plane is calculated for three fixed values of the product $mB = \pi \rho R^2 B$. Each curve is labelled by the corresponding mB value in units of 10^4 G-g/cm .

time of maximum compression, when the power of the PdV work done against the hot fuel is zero. In all practical formulas CGS units are used, and T is given in kiloelectronvolts.

The magnetic field B enters Eq. (16) through the coefficients f_α , κ_e and κ_i . The coefficients of electron, κ_e , and ion, κ_i , heat conduction have been calculated by using the Braginskii formulas [12], which for a plasma of hydrogen isotopes with $n_e = n_i = n$ take the form

$$\kappa_e = \frac{nT\tau_e}{m_e} \frac{11.92 + 4.664x_e^2}{3.7703 + 14.79x_e^2 + x_e^4} \quad (21)$$

$$\kappa_i = \frac{nT\tau_i}{m_i} \frac{2.645 + 2x_i^2}{0.677 + 2.70x_i^2 + x_i^4} \quad (22)$$

$$x_e = \omega_e \tau_e, \quad x_i = \omega_i \tau_i. \quad (23)$$

Here

$$\omega_e = \frac{eB}{m_e c}, \quad \omega_i = \frac{eB}{m_i c} \quad (24)$$

are, respectively, the electron and ion cyclotron frequencies, and

$$\tau_e = \frac{3m_e^{1/2} T^{3/2}}{4\sqrt{2}\pi e^4 n L_e}, \quad \tau_i = \frac{3m_i^{1/2} T^{3/2}}{4\sqrt{\pi} e^4 n L_i} \quad (25)$$

are the electron and ion collision times as defined in Ref. [12]. For the corresponding Coulomb logarithms, fixed values $L_e = 7$ and $L_i = 9$ were used, which roughly correspond to a DT plasma with $\rho = 1 \text{ g/cm}^3$, $T = 10 \text{ keV}$. Note that under the conditions of interest here the ion heat conduction is no less important than the electron one because in the strongly magnetized case, when $\omega_e \tau_e \gg 1$, $\omega_i \tau_i \gg 1$, we have $\kappa_e \ll \kappa_i$.

The fraction of the alpha particle energy, f_α , left in the DT region was evaluated from Eq. (15). For the alpha mean free path l_α we used the expression

$$l_\alpha = \frac{3}{4\sqrt{2}\pi} \frac{m_\alpha v_{\alpha 0} T^{3/2}}{Z_\alpha^2 e^4 n m_e^{1/2} L_\alpha} = 0.107 \frac{T_{\text{keV}}^{3/2}}{\rho L_\alpha} \text{ [cm]} \quad (26)$$

which accounts for the alpha stopping by the free plasma electrons at temperatures $T > 1 \text{ keV}$; the value of the Coulomb logarithm L_α was fixed at $L_\alpha = 7$.

The LW diagram shown in Fig. 3 has a clear physical meaning: for a target to ignite, the fuel parameters at stagnation must reach the domain $dT/dt > 0$. If the ignition domain is reached in the process of hydrodynamic implosion, the optimum ‘entry point’ corresponds approximately to the minimum of the triple product $\rho R T$, which occurs at $T = 6\text{--}8 \text{ keV}$ depending on the strength of the magnetic field. In this base version of the LW diagram for the magnetized fuel no second ignition island (as shown in Fig. 1 of Ref. [4]) appears at low ρR : the ‘standard’ ICF ignition region expands monotonically towards lower ρR as the parameter B/ρ is increased, namely, $(\rho R)_{\text{ign}} \propto (B/\rho)^{-1}$ in the limit of a strong field (this scaling is explained in the next section). Note that in the ideal case of a fully trapped magnetic field the ratio B/ρ is conserved in the process of cylindrical implosions, so that the point representing the current state of the imploding fuel in the $\rho R, T$ plane advances (as indicated by dashed arrows in Fig. 3) towards a stationary ignition boundary.

Alternative forms of the ignition curve parameter can be obtained by multiplying the ratio B/ρ by any combination of powers of T and ρR . Figure 4 shows a topologically different version of the LW diagram. Here each ignition boundary is calculated for a fixed value of the product mB , where $m = \pi \rho R^2$ is the fuel mass per unit cylinder length. For low values of mB , there are two disconnected ignition regions with $dT/dt > 0$, one at large ρR corresponding to the ICF ignition mode, and the other at low ρR corresponding to the ignition under external (magnetic, in particular) confinement. For $mB > 3 \times 10^4 \text{ G/g/cm}$

the two regions merge, and ignition becomes possible at any value of the fuel ρR , provided that a long enough confinement time is ensured. This type of LW diagram might be appropriate for situations when, for example,

- (a) One chooses a fixed value of the fuel mass m and studies the dependence of the ignition threshold on the magnetic field strength.
- (b) The experimental conditions impose a fixed upper limit on the maximum achievable value of the magnetic field B .

In the LW diagrams of Figs 3 and 4 no account was taken of the synchrotron radiation losses. Kilcrease and Kirkpatrick [13] have already argued that the synchrotron losses are not important in the MTF case. This is illustrated in Fig. 3 with the dotted curve calculated for $\rho = 1 \text{ g/cm}^3$, $B = 10^8 \text{ G}$ by adding the synchrotron loss term [13],

$$q_{\text{syn}} = 1.50 \times 10^6 T_{\text{keV}} B^2 \times (1 + 4.9 \times 10^{-3} T_{\text{keV}}) \text{ [erg g}^{-1} \text{ s}^{-1}] \quad (27)$$

to Eq. (16). Note that introduction of this term violates the similarity law which reduces the solution of the equation $dT/dt = 0$ to a one parameter family of curves in the $\rho R, T$ plane because, in contrast to the ratios q_{tn}/ρ , q_{br}/ρ and q_c/ρ , the ratio $q_{\text{syn}}/\rho \propto T B^2/\rho$ cannot be expressed as a function of the parameters T , ρR and B/ρ only.

4. Ignition criterion for the MTF mode

The well known ICF ignition criterion for the non-magnetized DT fuel is usually quoted as a lower bound on the fuel T and ρR values; for DT cylinders, as inferred from the $B = 0$ curve in Fig. 3, it reads

$$\begin{cases} T = 5\text{--}7 \text{ keV} \\ \rho R \geq 0.2 \text{ g/cm}^2. \end{cases} \quad (28)$$

The MTF ignition mode aims at igniting the DT fuel at ρR values considerably lower than the ICF threshold of $0.2\text{--}0.3 \text{ g/cm}^2$. Hence, the constraint on ρR should be replaced by another condition. We find this condition by taking a closer look at the thermal balance of stagnating fuel.

First of all, a necessary condition is that the thermonuclear alpha heating q_{tn} exceeds the

bremsstrahlung losses q_{br} . According to Eqs (18) and (19), this implies

$$f_\alpha > 3.8 \times 10^{-18} \frac{T_{keV}^{1/2}}{\langle \sigma v \rangle_{DT}}. \quad (29)$$

The function $T_{keV}^{1/2}/\langle \sigma v \rangle_{DT}$ has a minimum of $8.1 \times 10^{15} \text{ keV}^{1/2} \text{ s cm}^{-3}$ at $T = 40 \text{ keV}$. We, however, are interested in the temperature interval $T \approx 7\text{--}10 \text{ keV}$ (where the optimum ‘entry’ point into the ignition domain lies), for which Eq. (29) yields

$$f_\alpha > 0.25\text{--}0.1. \quad (30)$$

From Fig. 2 we infer that, in the limit of $R \ll l_\alpha$, inequality (30) implies a lower bound on the parameter

$$b = \frac{R}{r_{\alpha L}} > 1.5\text{--}1.0 \quad (31)$$

or, equivalently, a lower bound on the product BR . In other words, ignition in the MTF regime requires the 3.5 MeV alpha particles to be at least marginally magnetized, so that their Larmor radii be at least about equal to the hot fuel radius R .

The constraint (31) simplifies evaluation of the role of the heat conduction losses. For temperatures $T \gtrsim 6 \text{ keV}$ inequality (31) implies that the magnetization parameter for the plasma ions [12],

$$\omega_i \tau_i > \frac{0.015 \text{ g/cm}^2}{\rho R} \quad (32)$$

exceeds 1 for $\rho R \lesssim 0.01 \text{ g/cm}^2$. As a consequence, we can neglect the electron heat conduction because in the limit of strong magnetization the ratio of the two conductivities becomes

$$\frac{\kappa_e}{\kappa_i} = 2.33 \frac{m_i \omega_i^2 \tau_i}{m_e \omega_e^2 \tau_e} = 2.33 \sqrt{\frac{2m_e}{m_i}} \ll 1 \quad (33)$$

(here the electrons and ions are assumed to have equal temperatures and Coulomb logarithms). Adding the conduction cooling,

$$q_c = \frac{2\kappa_i T}{\rho R^2} = 1.145 \times 10^{24} \frac{\rho T_{keV}^{1/2}}{b^2} [\text{erg g}^{-1} \text{ s}^{-1}] \quad (34)$$

in the limit of $\omega_i \tau_i \gg 1$ to the ignition condition

$$q_{tn} > q_{br} + q_c \quad (35)$$

we obtain an inequality,

$$f_\alpha > 3.8 \times 10^{-18} \frac{T_{keV}^{1/2}}{\langle \sigma v \rangle_{DT}} \left(1 + \frac{3.68}{b^2} \right). \quad (36)$$

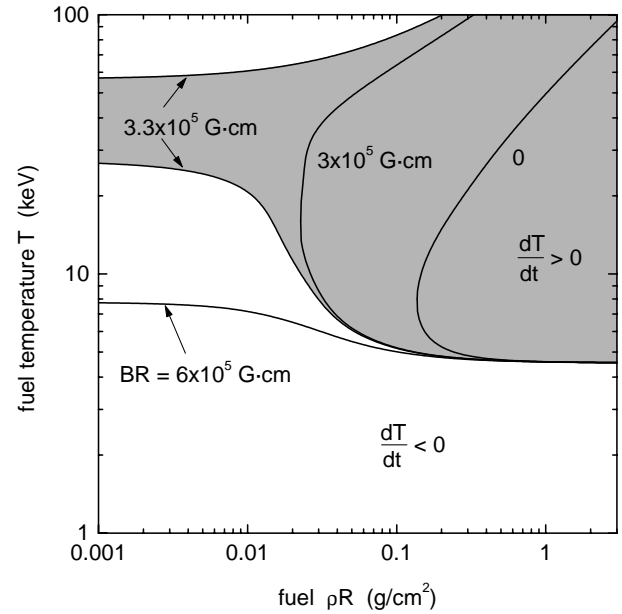


Figure 5. The BR form of the LW diagram: along each ignition curve the product BR is kept constant at the corresponding marked value.

In the limit of $R \ll l_\alpha$, when f_α becomes a function of b only in the relevant parameter range, inequality (36) can be resolved to yield

$$b > 2.3\text{--}1.5 \quad (37)$$

(for temperatures $T = 7\text{--}10 \text{ keV}$). Finally, we arrive at the following ignition criteria for the magnetized cylindrical targets:

$$\begin{cases} T = 7\text{--}10 \text{ keV} \\ BR \geq (6.5\text{--}4.5) \times 10^5 \text{ G cm} \end{cases} \quad (38)$$

which replaces the ICF criterion (28). Conditions (38) must be fulfilled in the DT fuel at stagnation if the ignition is to occur at a ρR value significantly below the ICF threshold of $0.2\text{--}0.3 \text{ g/cm}^2$. As one can infer from Fig. 2, the error introduced into the BR threshold by inaccuracy of the approximate formula (15) for $f_\alpha \approx 0.1\text{--}0.3$ is not large ($\approx 20\%$), and is comparable to the accuracy of the other assumptions made.

The lower bound on the BR product given by Eq. (38) is in perfect agreement with the numerical results for $B/\rho \gtrsim 10^8 \text{ G cm}^3/\text{g}$ shown in Fig. 3. It explains also the scaling $(\rho R)_{ign} \propto (B/\rho)^{-1}$ for the ignition threshold observed in Fig. 3. Note that inequality (36) implies that there is no regime with $q_c \gg q_{br}$: the bremsstrahlung is always at least comparable to (if not dominating over) the heat

conduction as the cooling mechanism near the ignition threshold of magnetized targets.

One can construct also an LW diagram by assuming the product BR to be constant along the ignition curves. Figure 5 shows what this diagram looks like. Its topology is intermediate between the two cases of Figs 3 and 4. The ignition domain $dT/dt > 0$ is always single connected, and for $BR < (BR)_* \approx 3.3 \times 10^5$ G cm it looks similar to the ignition region in Fig. 3. When the BR parameter exceeds the threshold value $(BR)_*$, the $dT/dt > 0$ region extends to infinitely small ρR and ignition becomes possible at any ρR value (in the absence of other possible limiting effects such as Compton or synchrotron cooling). It is seen also that for the practically interesting case of ignition temperatures around 10 keV the BR threshold is close to 6×10^5 G cm.

5. Summary and discussion

As already discussed in previous publications [2, 4], magnetization of thermonuclear fuel opens a possibility to ignite ICF targets in a new MTF mode which is characterized by strongly reduced fuel ρR values ($\ll 0.3$ g/cm²) as compared with those of the usual ICF case. In this article we have analysed the necessary conditions for achieving the MTF ignition in uniform DT cylinders with axial magnetic fields. As a first step, we calculate the energy fraction f_α deposited by the 3.5 MeV alpha particles in a cylindrical DT volume as a function of its ρR and the magnetic field strength B . An approximate formula for f_α is proposed, which agrees fairly well with the results of numerical simulations.

Having examined the thermal balance of stagnating DT cylinders, we find that the MTF ignition threshold corresponds to a lower limit on the product $BR \gtrsim 6 \times 10^5$ G cm, which replaces the lower limit on the fuel $\rho R \gtrsim 0.2\text{--}0.3$ g/cm² in the conventional ICF ignition criterion. The above constraint on the BR value has a simple physical meaning: to offset the plasma cooling by the bremsstrahlung and heat conduction, a large enough alpha energy fraction should be deposited in the fuel volume, which is possible only when the alpha Larmor radius becomes of the order of or smaller than the fuel radius R .

An important condition here is that the magnetic field lines are parallel to the surface of the igniting DT volume. Evidently, this is easier to arrange for a cylinder than for a sphere. If the magnetic field lines pierce the surface (as, for example, in the case of a DT sphere in a uniform magnetic field), even

an infinitely strong field (cf. Ref. [9]) cannot ensure ignition conditions in a DT volume with $R \ll l_\alpha$. In this respect the MTF ignition mode is similar to magnetic confinement fusion. We expect that in the case of spherical targets, once a magnetic field is created which is parallel to the surface of a DT sphere, the MTF ignition criterion should be very similar to the cylindrical case analysed here.

In our analysis no account has been taken of the finite time t_c of the inertial confinement. For a fuel volume with parameters ρ , T and R which is surrounded by a heavy cold liner of density ρ_l , the dwell time t_c of the stagnation phase scales as

$$t_c \propto R \left(\frac{\rho_l}{P} \right)^{1/2} \propto \frac{1}{\sqrt{T}} \left(\frac{\rho_l}{\rho} \right)^{1/2} \frac{m}{\rho R}. \quad (39)$$

One readily ascertains that the timescale for the development of a thermonuclear flare,

$$t_f \propto \frac{T}{\langle \sigma v \rangle_{DT}} \frac{1}{\rho} \propto \frac{T}{\langle \sigma v \rangle_{DT}} \frac{m}{(\rho R)^2} \quad (40)$$

increases faster than t_c as one fixes the fuel mass m and reduces the ignition ρR by magnetizing the fuel (even when the weak dependences of the factor $(\rho_l/\rho)^{1/2}$ on m and ρR are taken into account). Hence, so long as one stays within the context of ICF, the ρR ignition threshold in the MTF mode can be reduced by only a limited factor (of the order of 3–10), which is to be determined by the magnetohydrodynamics simulations. Ignition at still lower ρR values (provided that the BR parameter is sufficiently large) would only be possible under some non-inertial external (magnetic, for example) confinement.

Another important issue not addressed in this article is the finite cylinder length in realistic target configurations. Depending on a specific target design, the cylindrical section analysed in this work may only be an initiating (ignition) part of a more complex configuration (a possible scheme of such a cylindrical target that might be relevant to inertial fusion energy is given in Refs [5–7]). Clearly, the results of the present work will be applicable only when the length of the ignition section is large compared with its radius. Since heat conduction and alpha transport in the axial direction cannot be strongly inhibited by the axial magnetic field, one can expect that the lower limit on the fuel $\rho \Delta z$ should be of the order of the minimum ρR value in the non-magnetized case, i.e. $\rho \Delta z \gtrsim 0.3$ g/cm². The impact of non-cylindrical hydrodynamic perturbations at the ends of the ignition cylinder will be largely determined by specific features of the overall target design. If, however, the

ignition section is sufficiently long and the radial implosion is sufficiently fast, these perturbations are not expected to seriously distort the one dimensional results of the present work.

An interesting alternative to the quasi-uniform axial magnetization would be a cylinder with an azimuthal (ϕ) magnetic field. However, a detailed analysis of such a configuration in the context of MTF should involve more complex electrodynamics of the whole target and remains for future work. Note that the ϕ field must vanish on the cylinder axis, i.e. exactly where one expects an igniting hot core of magnetized fuel to be formed.

Finally, a remark on the possible role of Bohm diffusion. There are at least two arguments why Bohm diffusion should not affect noticeably the results of this work. The first is that the Bohm mechanism cannot be effective under the MTF conditions simply because the plasma to cyclotron frequency ratio is large, and the $\mathbf{E} \times \mathbf{B}$ drift in fluctuating \mathbf{E} fields has no time to manifest itself [4]. The second argument is that, even if the Bohm mechanism were operative, its effect near the MTF ignition threshold would be at most to make the electron heat conduction comparable to the ion heat conduction. Indeed, from Fig. 2 one infers that the product $\omega_i \tau_i \rho R$ has almost a constant value of 0.02–0.03 g/cm² at the ignition threshold. Hence, for feasible minimum ignition values of $\rho R \approx 0.01$ –0.03 g/cm² (cf. the previous paragraph), the plasma ions are only marginally magnetized, i.e. $\omega_i \tau_i \sim 1$. Then, the Bohm enhancement of the classical electron conductivity is by about a factor $\omega_e \tau_e = (m_i/2m_e)^{1/2} \omega_i \tau_i \sim (m_i/2m_e)^{1/2}$, which brings it to approximately the same level as the marginally magnetized ion conductivity that has already been accounted for.

Appendix

Alpha energy transport in the diffusion approximation

One of the approximate methods of describing the energy transport by 3.5 MeV alpha particles reduces to a diffusion equation,

$$\frac{\partial \mathcal{E}_\alpha}{\partial t} = \nabla \cdot (D_\alpha \nabla \mathcal{E}_\alpha) - G_\alpha \mathcal{E}_\alpha + \dot{n}_\alpha E_{\alpha 0} \quad (41)$$

for the volumetric energy density \mathcal{E}_α [erg/cm³] of the fast alphas [14, 15]. Here D_α and G_α are, respectively, the diffusion and dissipation coefficients, $\dot{n}_\alpha = n_{DN_T} \langle \sigma v \rangle_{DT}$ is the local alpha birth rate and

$E_{\alpha 0} = 3.5$ MeV. For the deceleration law given by Eqs (7) one calculates [14]

$$G_\alpha = 2\nu_\alpha \quad (42)$$

$$D_\alpha = \frac{v_{\alpha 0} l_\alpha}{18 + 2(\omega_\alpha/\nu_\alpha)^2}. \quad (43)$$

In Eq. (43) D_α is the diffusion coefficient across the magnetic field.

By solving Eq. (41) for a uniform stationary cylinder of radius R , one readily calculates the total alpha energy fraction deposited in the cylinder,

$$f_\alpha = 1 - \frac{2}{x_{\alpha d}} \frac{I_1 K_1}{I_0 K_1 + I_1 K_0} \quad (44)$$

$$= \begin{cases} \frac{1}{8} x_{\alpha d}^2 \left(1 + 4 \ln \frac{2}{\gamma x_{\alpha d}} \right), & x_{\alpha d} \ll 1 \\ 1 - \frac{1}{x_{\alpha d}} + O\left(\frac{1}{x_{\alpha d}}\right), & x_{\alpha d} \gg 1 \end{cases}$$

where

$$x_{\alpha d} = 2\sqrt{9 + (\omega_\alpha/\nu_\alpha)^2} \bar{R} \quad (45)$$

$I_n = I_n(x_{\alpha d})$ and $K_n = K_n(x_{\alpha d})$ are modified Bessel functions, $\gamma = \exp(C) = 1.781\dots$, and the dimensionless radius \bar{R} is defined in Eq. (5).

Generally, the diffusion approximation becomes asymptotically accurate in the limit of large ‘optical thicknesses’ ($\bar{R} \gg 1$) and smooth gradients. In our case, the source term \dot{n}_α has a step at the cylinder boundary $r = R$. Nevertheless, Eq. (44) reproduces exactly the asymptotic limit of $\bar{R} \gg 1$ for the quantity $1 - f_\alpha$ when $B = 0$ ($\omega_\alpha = 0$, $b = 0$), as one easily verifies by comparing Eq. (44) with Eq. (11). If we assume now that the second asymptote in Eq. (44) is exact in the limit of strong magnetization ($\omega_\alpha \gg \nu_\alpha \Leftrightarrow b \gg \bar{R}$) as well, and then demand that the approximate formula (15) conforms to this asymptote, we recover the numerical coefficient for the term $9b^2$ in Eq. (15b).

References

- [1] Sweeney, M.A., Farnsworth, A.V., Jr., Nucl. Fusion **21** (1981) 41.
- [2] Lindemuth, I.R., Kirkpatrick, R.C., Nucl. Fusion **23** (1983) 263.
- [3] Jones, R.D., Mead, W.C., Nucl. Fusion **26** (1986) 127.
- [4] Kirkpatrick, R.C., Lindemuth, I.R., Ward, M.S., Fusion Technol. **27** (1995) 201.
- [5] Churazov, M.D., Sharkov, B.Yu., Zabrodina, E.A., Fusion Eng. Des. **32&33** (1996) 577.

- [6] Churazov, M.D., Aksenov, A.G., Krasnoborov, N.A., Zabrodina, E.A., Nucl. Instrum. Methods Phys. Res. A **415** (1998) 144.
- [7] Basko, M., Inertial Confinement Fusion with Magnetized Fuel in Cylindrical Targets, Rep. EUR-CEA-FC-1645, CEA Cadarache Saint Paul-lez-Durance (1998).
- [8] Fraley, G.S., Linnebur, E.J., Mason, R.J., Morse, R.L., Phys. Fluids **17** (1974) 474.
- [9] Gus'kov, S.Yu., Rozanov, V.B., Trebuleva, L.E., Kvantovaya Elektron. **11** (1984) 1575 [English translation: Sov. J. Quantum Electron. **14** (1984) 1062].
- [10] Krokhin, O.N., Rozanov, V.B., Kvantovaya Elektron. **4** (1972) 118 [English translation: Sov. J. Quantum Electron. **2** (1973) 393].
- [11] Lindl, J.D., in Inertial Confinement Fusion (Proc. Course and Workshop Varenna, 1988), Editrice Compositori, Bologna (1989) 617.
- [12] Braginskii, S.I., in Reviews of Plasma Physics, Vol. 1, Consultants Bureau, New York (1965) 205.
- [13] Kilcrease, D.P., Kirkpatrick, R.C., Nucl. Fusion **28** (1988) 1465.
- [14] Liberman, M.A., Velikovich, A.L., J. Plasma Phys. **31** (1984) 369.
- [15] Basko, M.M., Fiz. Plazmy **13** (1987) 967 [English translation: Sov. J. Plasma Phys. **13** (1987) 558].

(Manuscript received 21 July 1999)

Final manuscript accepted 19 October 1999)

E-mail address of M.M. Basko: basko@vitep5.itep.ru

E-mail address of A. Kemp: kemp@mpq.mpg.de

Subject classification: L0, It